Letters

Characterization of Three-Phase Common-Mode Chokes at High Frequencies

Carlos Domínguez-Palacios, Joaquin Bernal Mendez, *Senior Member, IEEE*, and Maria Angeles Martin Prats, *Senior Member, IEEE*

***Abstract*—This letter presents a method to characterize three-phase common-mode chokes at high frequencies. By performing a modal analysis of a high-frequency circuit model of the common mode choke regarded as a six-ports device, we demonstrate that when excited in a simple setup, the common-mode and differential-mode resonances of the three windings of the common mode choke can be plainly observed. This permits us to predict the response of the common mode choke to common mode and differential mode excitations with a simple measurement, i.e., two different setups are not required. Also it allows us to develop a method to determine the high-frequency parameters of the circuit model from the result of this simple measurement. Different commercial three-phase common-mode chokes have been measured and the predicted performance of the model has been compared with measured responses.**

***Index Terms*—Circuit modeling, electromagnetic compatibility, electromagnetic interference, filtering.**

I. Introduction

COMMON mode chokes (CMC) are key components of electromagnetic interference (EMI) filters intended to limit common mode (CM) emissions, although they also affect differential mode (DM) currents at high frequencies [1]. It is well known that the performance of CMCs at high frequencies is undermined by parasitic effects such as parasitic parallel capacitances between windings [1], [2]. Since electromagnetic compatibility (EMC) standards impose emissions limits at high frequencies and because modern trends in the design of power converters are toward the use of higher frequencies to increase power density, an accurate characterization of the response of the components of the EMI filter, such as CMCs, at high frequencies is becoming a fundamental step in the design process of power converters [3]–[5].

A method to characterize two-phase CMCs (2P-CMC) at high frequencies has been described previously in [6]. In that work, it is demonstrated that due to the special symmetry of this device, a single measurement performed with a spectrum analyzer (SA) with tracking generator (TG) on a simple setup of the CMC, referred to as an open circuit (OC) setup, makes it possible to determine the response of the 2P-CMC to both CM and DM excitations.

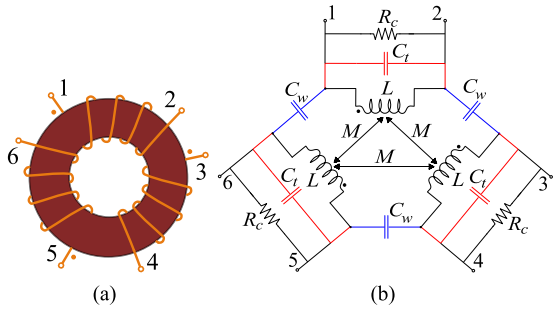

Fig. 1. Representation and circuit model of a 3P-CMC. (a) Three-phase common mode choke. (b) High-frequency circuit model of the 3P-CMC.

In high power systems, three-phases CMCs (3P-CMC) are usually employed to reduce CM noise [7]. A 3P-CMC comprises three coupled windings in instead of two, as shown in Fig. 1(a). This figure also shows a typical high-frequency model of the 3P-CMC that includes capacitive parasitics. In this letter, we extend the modal analysis previously developed for 2P-CMCs to analyze the circuit model of a 3P-CMC, which here is treated as a six-ports network. This analysis demonstrates that although the 3P-CMC features five natural modes with nonzero admittance instead of the three modes that are found for a 2P-CMC [6], and despite the fact that the 3P-CMC lacks the plane of symmetry of the 2P-CMC, these modes remain as either CM or DM. As a consequence, when excited in a simple OC setup, the transmission coefficient of a 3P-CMC must show two resonance dips that correspond to CM and DM excitations of the 3P-CMC. This establishes a parallel with the case of 2P-CMCs that in principle is not obvious and which makes it possible to evaluate the high-frequency response of a 3P-CMC for both CM and DM excitations with a single measurement instead of using two different setups to excite CM and DM modes [4], [6]. Moreover, from the analysis presented in this letter, it is possible to obtain an analytical expression for the transmission coefficient of a 3P-CMC connected in the OC setup. This allows the development of an efficient method for extraction of the parasitic

Manuscript received November 22, 2017; revised December 11, 2017; accepted January 11, 2018. Date of publication January 14, 2018; date of current version April 20, 2018. This work was supported by the Spanish Ministerio de Economía y Competitividad under project TEC2014-54097-R. *(Corresponding author: Joaquin Bernal Mendez.)*

C. Domínguez-Palacios and M. M. Prats are with the Department of Ingeniería Electrónica, Universidad de Sevilla, Sevilla 41092, Spain (e-mail: cardompal@alum.us.es; mmprats@us.es).

J. B. Mendez is with the Department of Física Aplicada III, Universidad de Sevilla, Sevilla 41092, Spain (e-mail: jbmendez@us.es).

Color versions of one or more of the figures in this letter are available online at http://ieeexplore.ieee.org.

Digital Object Identifier 10.1109/TPEL.2018.2793798

TABLE I
MODES OF THE CIRCUIT OF FIG. 1(B), WHERE $B = Y_{\rm DM}/(2Y_w)$ AND $A = \sqrt{1 + B(B-1)}$

Mode type	Excitation\eigenvector	Admittance\eigenvalue	
C	$v_C = [1, 1, 1, 1, 1, 1]$		$Y_{\rm C} = 0$
CM	$v_{\rm CM} = [-1, 1, -1, 1, -1, 1]$		$Y_{\rm CM} = 2\left(jw(C_t + C_w) + \frac{1}{jw(L+2M)}\right)$
DM	$v_{DM1} = [A, -1 + B, -A, -B, 0, 1]$	$\lambda_{DM_{12}} = (2Y_w(1-A) + Y_{\rm DM})/2$	$Y_{\rm DM} = 2\left(jwC_t + \frac{1}{jw(L-M)}\right)$
	$v_{DM2} = [-B, -A, -1 + B, A, 1, 0]$		
	$v_{DM3} = [-A, -1 + B, A, -B, 0, 1]$	$\lambda_{DM_{34}} = (2Y_w(1+A) + Y_{\rm DM})/2$	$Y_w = jwC_w$
	$v_{DM4} = [-B, A, -1 + B, -A, 1, 0]$		

elements of the model of the 3P-CMC, which only require the measured OC curve as an input.

The accuracy and scope of the method proposed here are studied by extracting the parasitic parameters for several commercial 3P-CMCs and by comparing the attenuation as predicted by the circuit model with measured attenuations.

II. ANALYSIS

Fig. 1(b) shows a lumped-element circuit model of a 3P-CMC, which can be regarded as a generalization of the model proposed in [6] for the 2P-CMC. The model includes three equal magnetically coupled windings that determine the low-frequency response of the choke. Also, parallel winding capacitances (C_t) and inter-winding capacitances (C_w) have been added to account for the electrical couplings that determine the high-frequency behavior of the 3P-CMC [7]. In this model, losses within the magnetic material are accounted for by placing resistors (R_c) in parallel with the coupled inductors. Note that this model disregards additional capacitive couplings that might appear between nonadjacent winding nodes. This approximation greatly simplifies the problem and can be justified by the fact of the physical construction of most practical 3P-CMCs, where distance between nonadjacent nodes are considerably larger than distance between adjacent nodes.

Considering the circuit in Fig. 1(b) as a six-ports network, this model of the 3P-CMC can be characterized by a 6×6 admittance matrix $[Y]$, that relates currents and voltages (referred to ground) in the six ports. This admittance matrix can easily be obtained by circuit analysis. We can perform a modal analysis by calculating the voltage eigenvectors (modes) that diagonalize [Y]. In this way, the response of the 3P-CMC to a particular excitation can be expressed in terms of the admittances (eigenvalues) of the modes excited for that particular connection of the 3P-CMC. It is interesting to note that for a 2P-CMC both the CM and the DM appear directly as two of the four natural modes of the circuit [6]. For these CM and DM modes, the admittances corresponds to those of a parallel LCR connection, where the inductive component is $L + M$ for the CM and $L - M$ (the leakage inductance) for the DM, as expected. These CM and DM modes correspond to even and odd modes with respect to the plane of symmetry of the 2P-CMC [6]. An analysis of the 3P-CMC of Fig. 1(b), which lacks this plane of symmetry, reveals that in this case we have six modes. The eigenvectors and eigenvalues (admittances) of these modes are

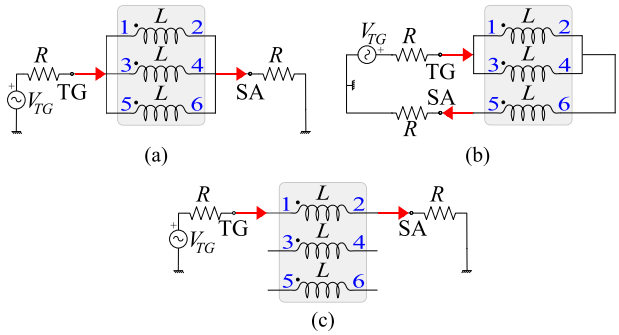

Fig. 2. Experimental setups for measuring the transmission coefficient of a 3P-CMC with a spectrum analyzer (SA) with tracking generator (TG). (a) Common mode (CM) setup. (b) Differential mode (DM) setup. (c) Open circuit (OC) setup.

listed in Table I. It can be seen that there exist a C mode, which corresponds to a simultaneous excitation of all the terminals with the same voltage, and whose admittance is $Y_C = 0$ because we have disregarded the parasitic capacitance to ground, which is a reasonable approximation [6], [7]. Also, there exist a CM mode corresponding to a excitation of all the windings with the same voltage drop. The inductive component of the admittance $Y_{\rm CM}$ of this mode is $L + 2M$, i.e., the common mode inductance of the 3P-CMC [7]. The remaining four modes can be identified as differential modes because their admittances are expressed in terms of $Y_{\rm DM}$, whose inductive component is the leakage inductance $L - M$. Also, note that for these four modes the sum of the voltage drops applied to the three windings is zero: $(V_1 - V_2) + (V_3 - V_4) + (V_5 - V_6) = 0$ and, therefore, ideally the magnetic flux in the core due to currents flowing in the three identical windings is zero, which is the general condition for DM [7].

The attenuation that a 3P-CMC provides for a CM or DM signal can be determined by measuring the magnitude of the transmission coefficient, $|S_{21}|$, when the 3P-CMC is connected as indicated, respectively, in Fig. 2(a) and (b). An SA with TG or a vector network analyzer (VNA) can be used to this end. Alternatively, as we will see, the simple setup here referred to as OC setup, shown in Fig. 2(c), can be used to extract valuable information about both the CM and the DM responses of a 3P-CMC with a single measurement.

From the modal analysis summarized in Table I, it is possible to obtain analytical expressions for the transmission coefficients

TABLE II
TRANSMISSION COEFFICIENTS AND FREQUENCIES OF RESONANCE FOR THE SETUPS OF FIG. 2

Setup	Transmission coefficient	Frequencies of resonance
CM	$S_{21}^{\mathrm{CM}} = \frac{3RY_{\mathrm{CM}}}{3RY_{\mathrm{CM}}+1}$	$\omega_{\mathrm{CM}} = \frac{1}{\sqrt{(C_t+C_w)(L+2M)}}$
DM	$S_{21}^{\mathrm{DM}} = \frac{2RY_{\mathrm{DM}}+4RY_w}{2RY_{\mathrm{DM}}+4RY_w+3}$	$\omega_{\mathrm{DM}} = \frac{1}{\sqrt{(C_t+C_w)(L-M)}}$
OC	$S_{21}^{\mathrm{OC}} = \frac{2RY_{\mathrm{OC}}}{2RY_{\mathrm{OC}}+1}$	$\omega_{\mathrm{OC1}} = \omega_{\mathrm{CM}}$
		$\omega_{\mathrm{OC2}} = \frac{1}{\sqrt{C_t(L-M)}}$

TABLE III
3P-CMCS ANALYZED IN THIS LETTER

Manufacturer	Part number	Inductance (mH)
EPCOS	B82747S4303A041	0.82
EPCOS	B82747E6353A040	1
EPCOS	B82747S4423N020	1.5
EPCOS	B82746S4103A02	1.7
EPCOS	B82746S4143A040	3.2
WÜRTH ELEKTRONIK	744835034160	3.4
WÜRTH ELEKTRONIK	744838040400	4

corresponding to the three setups of Fig. 2. These transmission coefficients along with their frequencies of resonance, obtained from the condition $S_{21} = 0$ for the lossless case ($R_c = \infty$), are given in Table II as functions of the Y_{CM} and Y_{DM} admittances defined in Table I. In the expressions in Table II, R stands for the resistances of the output and input ports of the SA+TG or VNA (usually $R = 50\ \Omega$). Also, the Y_{OC} admittance in that table is defined as follows:

$$Y_{\mathrm{OC}} = \frac{3Y_{\mathrm{CM}}Y_{\mathrm{DM}}}{4Y_{\mathrm{CM}} + 2Y_{\mathrm{DM}}}. \tag{1}$$

Table II shows that Y_{CM} appears in the expression of S_{21}^{CM} but not in S_{21}^{DM}. Also, Y_{DM} appears in S_{21}^{DM} but not in S_{21}^{CM}. This means that the DM setup only excites the DM modes of the 3P-CMC and the CM setup only excites the CM mode, as expected. Interestingly, both Y_{CM} and Y_{DM} appear in S_{21}^{OC} through Y_{OC} (1). This equation reveals that Y_{OC} can be regarded as the result of a connection in series of two impedances that are directly proportional to Y_{CM} and Y_{DM}. Consequently, and because the resonant condition $S_{21}^{\mathrm{OC}} = 0$ translates into $Y_{\mathrm{OC}} = 0$, this gives in the OC setup two frequencies of resonance given by the two conditions: $Y_{\mathrm{CM}} = 0$ and $Y_{\mathrm{DM}} = 0$. Physically, this means that 3P-CMC excited in the OC setup will first resonate with currents flowing in CM (inductance $L + 2M$ in parallel with $C_t + C_w$) at a frequency ω_{CM} and it will then also resonate at a higher frequency (ω_{OC2} in Table II) with currents flowing in DM (inductance $L - M$ in parallel with C_t). This analysis demonstrates that, in spite of the differences between the modes and the transmission coefficients found for a 3P-CMC when compared with a 2P-CMC [6], the main features of the response to an OC excitation are similar. This interesting result can then be exploited in a similar manner. First, key features of the attenuation provided by a 3P-CMC both for CM noise and for DM noise can be predicted by a simple inspection of the measured $|S_{21}^{\mathrm{OC}}|$. Second, the measured $|S_{21}^{\mathrm{OC}}|$ curve can be used to extract all the parameters of the circuit model of the 3P-CMC.

In this letter, we have adapted the method of extraction of parameters from the frequencies of resonance of S_{21}^{OC} originally developed for 2P-CMCs [6] to deal with the 3P-CMC case. Additionally, in order to investigate whether a more advanced search approach can further improve the results of this method, we have implemented an alternative technique of extraction of parameters that makes use of genetic algorithms (GA) to find a set of parasitic parameters for the circuit in Fig. 1(b) that fits the measured S_{21}^{OC} curve. The higher computational effort typically associated with evolutionary search algorithms is not an issue in this case due to the availability of analytical expressions for S_{21}^{OC} (Table II) in terms of the parameters of the circuit.

III. RESULTS

To validate the previous analysis, we have measured the commercial 3P-CMCs listed in Table III excited in the CM, DM, and OC setups of Fig. 2. We have confirmed that in all the cases, the S_{21}^{OC} exhibits the two resonances predicted by our analysis of Section II and that the first resonance coincides with that observed in S_{21}^{CM}, whereas the resonance at higher frequency is very close to that of S_{21}^{DM}. As an example, Fig. 3 shows the measured $|S_{21}|$ for the 3P-CMC specified in the caption of the figure when connected in the OC, CM, and DM setups. By comparing these measured curves, it can be concluded that S_{21}^{OC} alone allows the determination of where the 3P-CMC resonates in CM and the frequency range where it behaves capacitively (thus exhibiting decreasing attenuation with increasing frequency). Also, the measured S_{21}^{OC} informs us about the range of frequencies where the 3P-CMC provides a significant attenuation of the DM noise. To ensure that the approach proposed here is able to provide an accurate circuit model of this 3P-CMC throughout a sufficiently broad frequency range, we have obtained the parameters of the high-frequency circuit model of the 3P-CMC of Fig. 1(b) from the measured $|S_{21}^{\mathrm{OC}}|$ of Fig. 3(a). To do this, we have used both an algorithm that makes use of the frequencies of resonances of $|S_{21}^{\mathrm{OC}}|$ [6] and a GA. Results provided by these two methods are quite similar in this case. Parameters obtained with the GA are given in Table IV. We have inserted these parameters into the analytical expressions of the S_{21} coefficients of Table II to calculate the attenuation predicted by the circuit model for this 3P-CMC. Fig. 3 shows that measured and calculated curves agree very closely, which proves that the circuit model provides a good approximation for the attenuation of this 3P-CMC both in CM and in DM throughout a wide frequency range.

In some particular cases, the rapid rate of change of the permeability of the core of the CMC with frequency can make it difficult to find a good approximation of the CMC with the proposed circuit model [6]. To show an example of this, Fig. 4 shows the measured and calculated $|S_{21}^{\mathrm{OC}}|$ for the 3P-CMC listed as EPCOS B82746S4143A040 in Table III. Fig. 4 shows that the complex behavior of this 3P-CMC can only be approximately fitted by the GA (parameters given in

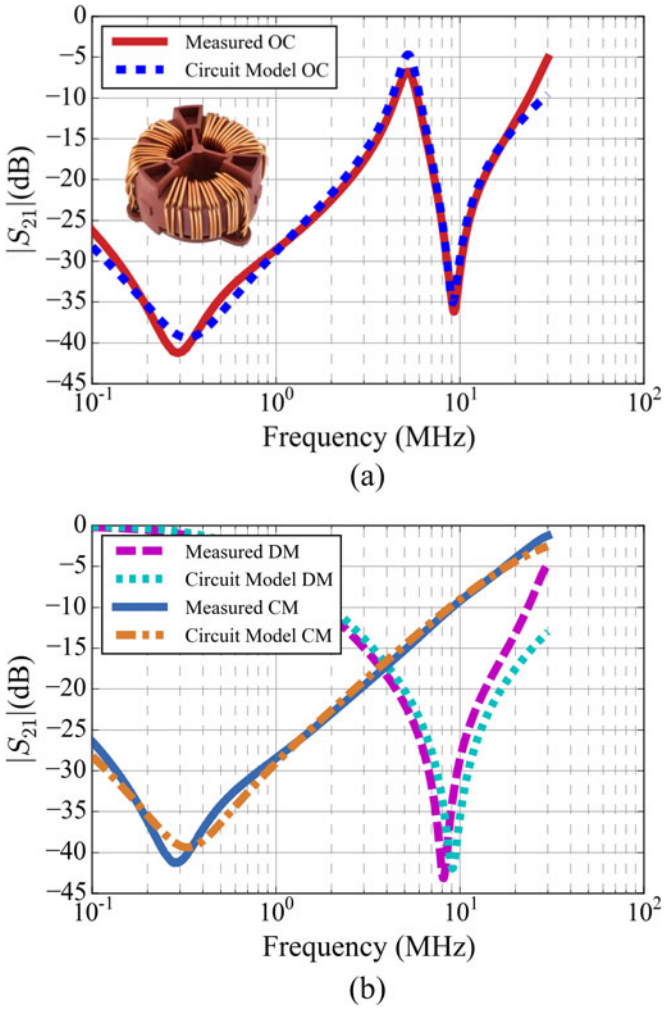

Fig. 3. Measured and approximated $|S_{21}|$ curves for the 3P-CMC shown in the upper figure and listed as WÜRTH ELEKTRONIK 744835034160 (3.4 mH) in Table IV. (a) Open circuit (OC). (b) Common mode (CM) and differential mode (DM).

TABLE IV
PARAMETERS EXTRACTED FROM TWO OF THE 3P-CMCS OF TABLE III

Parameter	WÜRTH ELEKTRONIK 744835034160	EPCOS B82746S4143A040
$L+2M$ (mH)	11.5	17.5
$L-M$ (μH)	15.1	7.98
C_t (pF)	20.3	6.66
C_w (pF)	0.056	0.89
R_1 (kΩ)	34.6	21.0
R_2 (kΩ)	9.65	6.56

Table IV). It is worth pointing out that the adaptation to the 3P-CMC case of the algorithm proposed in [6] is not able to provide an approximated $|S_{21}^{\mathrm{OC}}|$ curve in this case. This is due to the tight constraint imposed by this algorithm, which tries to force the $|S_{21}^{\mathrm{OC}}|$ curve of the circuit model to have exactly the same frequencies of resonance as the measured curve. Therefore, it can be concluded that the use of advanced search algorithms is advisable in order to to deal with 3P-CMCs

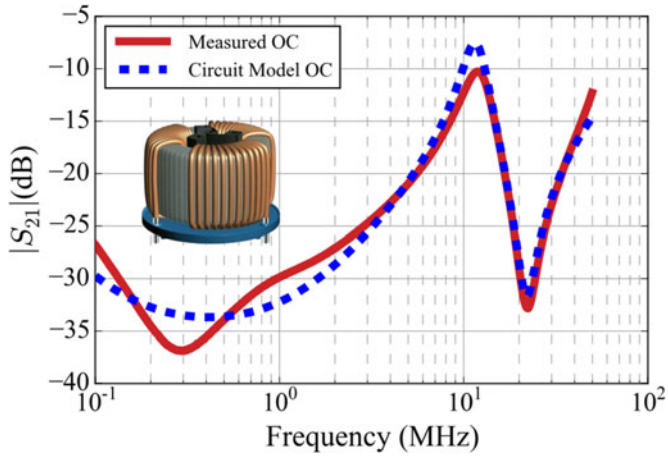

Fig. 4. Measured and approximated $|S_{21}|$ curves for the 3P-CMC shown in the figure and listed as EPCOS B82746S4143A040 (3.2 mH) in Table IV.

with complicated behaviors. Although in those cases, the limitations of the circuit model does not allow us to find a set of parameters that perfectly mimics the response of the 3P-CMC, approximated results can still be useful. Moreover, note that irrespective of the existence of a simple circuit that can approximate the response of the 3P-CMC for CM and DM, the actual response of the 3P-CMC can equally be ascertained from inspection of the measured $|S_{21}^{\mathrm{OC}}|$. This can be useful to aid prompt component selection.

IV. CONCLUSION

This letter presents a method to characterize and predict the response of a 3P-CMC at high frequencies. We perform a modal analysis of the high-frequency circuit model of a 3P-CMC regarded as a six-ports network. This allows us to demonstrate that when excited in a specific simple configuration (OC setup), the response of the 3P-CMC contains both the differential mode and the common mode natural responses of the 3P-CMC, each one dominating and giving rise to resonant behaviors in different frequency ranges. In that sense, a significant contribution of this letter is to demonstrate that 3P-CMCs, which in principle are more complex and lack the plane of symmetry of 2P-CMCs, have a behavior similar to that already reported for 2P-CMCs and that consequently, the measurement of the transmission coefficient of the 3P-CMC in the OC setup makes it possible to evaluate the response of the 3P-CMC both for CM and DM signals at the same time by using the results of a single measurement in a specific simple setup. Moreover, since the modal analysis proposed in this letter makes it possible to obtain a closed-form expression for the transmission coefficient of the 3P-CMC in the OC setup, we have shown that, as an alternative to the use of a method based on the frequencies of resonance, a search algorithm can be used to efficiently extract the parameters of the circuit model of the 3P-CMC from the measurement performed in the OC setup. We have measured and extracted the parameters of the high-frequency circuit for several commercial 3P-CMCs, generally finding good agreement between measured and predicted responses of the 3P-CMCs. Our results show that

the method of extracting parameters presents some limitations when dealing with 3P-CMCs with a high rate of change of the permeability of the core against frequency due to the fact that this effect is poorly accounted for by the high-frequency circuit model of the 3P-CMC.

REFERENCES

[1] C. R. Paul, *Introduction to Electromagnetic Compatibility*. Hoboken, NJ, USA: Wiley, 2006.

[2] S. Wang, F. C. Lee, and J. D. van Wyk, "Design of inductor winding capacitance cancellation for EMI suppression," *IEEE Trans. Power Electron.*, vol. 21, no. 6, pp. 1825–1832, Nov. 2006.

[3] M. Kovacic, Z. Hanic, S. Stipetic, S. Krishnamurthy, and D. Zarko, "Analytical wideband model of a common-mode choke," *IEEE Trans. Power Electron.*, vol. 27, no. 7, pp. 3173–3185, Jul. 2012.

[4] I. Stevanovic, S. Skibin, M. Masti, and M. Laitinen, "Behavioral modeling of chokes for EMI simulations in power electronics," *IEEE Trans. Power Electron.*, vol. 28, no. 2, pp. 695–705, Feb. 2013.

[5] I. F. Kovacevic, T. Friedli, A. M. Musing, and J. W. Kolar, "3-D electromagnetic modeling of parasitics and mutual coupling in EMI filters," *IEEE Trans. Power Electron.*, vol. 29, no. 1, pp. 135–149, Jan. 2014.

[6] C. Dominguez-Palacios, J. Bernal, and M. M. Prats, "Characterization of common mode chokes at high frequencies with simple measurements," *IEEE Trans. Power Electron.*, to be published. [Online]. Available: http://ieeexplore.ieee.org/document/7984867/

[7] M. L. Heldwein, L. Dalessandro, and J. W. Kolar, "The three-phase common-mode inductor: Modeling and design issues," *IEEE Trans. Ind. Electron.*, vol. 58, no. 8, pp. 3264–3274, Aug. 2011.